

Energy transfer mechanisms in compressible two-phase turbulent flows

By L. H. Hatashita[†], N. Tonicello[‡] AND S. S. Jain[†]

In this work, simulations of compressible two-phase turbulence are performed to study the fundamental characteristics of energy transfer in this unexplored regime. A decaying homogeneous isotropic turbulence in the presence of a drop of unity density and viscosity ratio, i.e., the same fluids, with a low-enough turbulent Weber number to avoid breakup is simulated. Explicit filtering is performed on highly resolved direct numerical simulation data to characterize resolved kinetic energy transfer terms and exchange between the resolved and sub-grid scales. In agreement with compressible single-phase cases, a correlation between backscatter and expansion regions is observed for higher-turbulence Mach numbers, and this phenomenon is strengthened near the interface. We hypothesize that the dilatational velocity also interacts with the interface, resulting in changes in the surface area and thus surface energy. This dilatational interaction between the kinetic and surface energies—dilatational surface tension power—is potentially responsible for the enhanced backscatter at the interface.

1. Introduction

Bubble- and drop-laden turbulent flows are ubiquitous in nature and industrial applications. In the compressible regime, cooling and propulsion systems are some examples. From a design and modeling perspective, accurate simulations require proper description of the flow physics. Thus, a fundamental understanding of the turbulence physics in the compressible regime and in the presence of material interfaces is imperative.

With the increase in computational resources, more complex geometries and partially scale-resolving simulation approaches, such as large-eddy simulations (LES), have received more attention. In LES, the phenomenon of kinetic energy backscatter, also known as the reverse energy cascade, has been extensively studied over the past few decades (Piomelli *et al.* 1991; Domaradzki *et al.* 1993; Kerr *et al.* 1996). By explicitly filtering direct numerical simulations (DNS) data, we can directly assess the contributions of sub-grid scales (SGS) to kinetic energy transfer via what is commonly known as *a-priori* analysis. Piomelli *et al.* (1991) initially demonstrated a predominance of forward energy cascade, as first proposed by Richardson (1922) and later formalized by Kolmogorov (1941), for 3D turbulence. However, their findings also revealed significant backscatter events, where small scales act as a source of kinetic energy for larger scales. Subsequent studies have confirmed the presence of backscatter in various applications in turbulent flows (O'Brien *et al.* 2014; Livescu & Li 2017; Wang *et al.* 2018).

Both *a-priori* and *a-posteriori* analyses of turbulent flows have been extended to more complex conditions, such as reactive and compressible flows, where thermodynamics plays a crucial role in the total energy balance. As a result, the description of energy transfers in

[†] Flow Physics and Computational Science Lab, Georgia Institute of Technology

[‡] MathLab, International School for Advanced Studies, Italy

turbulence has evolved from focusing solely on kinetic energy to incorporating more generalized forms that include internal energy. This shift has led to in-depth studies of the interaction between kinetic and internal energy, particularly examining pressure-dilatation work as the main mechanism for conversion between these energy forms (Livescu *et al.* 2002; Aluie 2013; Tonicello *et al.* 2022).

In the present work, the aim is to further extend our comprehension of inter-scale kinetic energy transfers to compressible two-phase flows. In addition to the complexity related to nonnegligible compressibility effects on turbulence, the influence of surface tension energy, which nonlinearly interacts with the other two main forms of energy (kinetic and internal), is also considered.

Previous work on *a-priori* analyses of turbulent two-phase flows (Labourasse *et al.* 2007; Toutant *et al.* 2008; Klein *et al.* 2019) explored the interaction between turbulence and surface tension in the incompressible regime, with a focus toward model development. The inclusion of compressibility effects, however, is still widely unexplored. The present work aims to give a more complete picture of the interactions between turbulence, surface tension effects, and compressibility using DNS of compressible two-phase isotropic turbulence. Although backscatter events have been observed in two-phase turbulent flows (Labourasse *et al.* 2007), they were in the context of 2D incompressible simulations. The analyses proposed in this work, instead, are fully 3D and also include the effects of compressibility. Different behaviors may be expected in this scenario. Ultimately, such information regarding the fundamental physics of the problem can lead to further improvements of the current state of the art regarding LES closure models for compressible two-phase flows.

The remainder of this report is structured as follows. In Section 2, the formulation and computational setup are briefly outlined. Section 3 is devoted to analyzing the terms in the resolved kinetic energy equation and their cross correlations. Finally, conclusions are drawn in Section 4.

2. Formulation and setup

In this work, for accurate simulations of compressible two-phase flows, we use a five-equation diffuse-interface model (Jain *et al.* 2020) with an accurate conservative diffuse-interface/phase-field method for interface capturing (Jain 2022) and a localized artificial-viscosity approach for capturing shocks and contact discontinuities (Jain *et al.* 2024). The system of conservation equations for volume fraction, mass of each phase, momentum, and total energy can be written as

$$\frac{\partial \phi_1}{\partial t} + \frac{\partial u_j \phi_1}{\partial x_j} = (\phi_1 + \zeta) \frac{\partial u_j}{\partial x_j} + \frac{\partial a_{1j}}{\partial x_j} + \frac{\partial}{\partial x_j} \left(D^* \frac{\partial \phi_1}{\partial x_j} \right), \quad (2.1)$$

$$\frac{\partial \rho_l \phi_l}{\partial t} + \frac{\partial u_j \rho_l \phi_l}{\partial x_j} = \frac{\partial R_{lj}}{\partial x_j} + \frac{\partial}{\partial x_j} \left(D^* \frac{\partial \rho_l \phi_l}{\partial x_j} \right), \quad l = 1, 2, \quad (2.2)$$

$$\begin{aligned} \frac{\partial \rho u_i}{\partial t} + \frac{\partial \rho u_i u_j}{\partial x_j} + \frac{\partial p}{\partial x_i} &= \frac{\partial u_i f_j}{\partial x_j} + \frac{\partial \Sigma_{ij}}{\partial x_j} + \sigma \kappa \frac{\partial \phi_1}{\partial x_i} + \rho g_i \\ &+ \frac{\partial}{\partial x_j} \left(D^* u_i \frac{\partial \rho}{\partial x_j} \right) + \frac{\partial}{\partial x_j} \left(\beta^* \frac{\partial u_k}{\partial x_k} \delta_{ij} \right), \end{aligned} \quad (2.3)$$

$$\begin{aligned} \frac{\partial E}{\partial t} + \frac{\partial (E + p) u_j}{\partial x_j} = & \frac{\partial \Sigma_{ij} u_i}{\partial x_j} + \frac{\partial k f_j}{\partial x_j} + \sum_{l=1}^2 \frac{\partial \rho_l h_l a_{lj}}{\partial x_j} + \sigma \kappa u_i \frac{\partial \phi_1}{\partial x_i} + \rho u_i g_i \\ & + \frac{\partial}{\partial x_j} \left[D^* \frac{\partial \rho}{\partial x_j} \left(\frac{u_k u_k}{2} \right) \right] + \frac{\partial}{\partial x_j} \left(D^* \frac{\partial \rho e}{\partial x_j} \right) + \frac{\partial}{\partial x_j} \left(\beta^* \frac{\partial u_k}{\partial x_k} \delta_{ij} u_i \right), \end{aligned} \quad (2.4)$$

where ϕ_l is the volume fraction of phase l that satisfies the condition $\sum_{l=1}^2 \phi_l = 1$; ζ is the asymptotic reduction variable for the five-equation model (zero herein); ρ_l is the density of phase l ; ρ is the total density, defined as $\rho = \sum_{l=1}^2 \rho_l \phi_l$; u_i is the velocity; p is the pressure; e is the specific mixture internal energy, which can be computed from the specific internal energy of phase l , e_l , as $\rho e = \sum_{l=1}^2 \rho_l e_l$; $k = u_i u_i / 2$ is the specific kinetic energy; and $E = \rho(e + k)$ is the total energy of the mixture per unit volume. Viscous stresses Σ_{ij} are taken to be Newtonian, assuming Stokes hypothesis. In Eq. (2.4), $h_l = e_l + p / \rho_l$ represents the specific enthalpy of phase l and can be expressed in terms of ρ_l and p using the stiffened-gas equation of state as

$$h_l = \frac{(p + \pi_l) \gamma_l}{\rho_l (\gamma_l - 1)}. \quad (2.5)$$

In Eqs. (2.1)-(2.4), σ is the surface tension coefficient, $\kappa = -\partial n_{1i} / \partial x_i$ is the curvature of the interface, n_{li} is the normal vector of the interface for phase l (in two-phase, $n_{1i} = -n_{2i}$), and a_{li} is the volumetric interface regularization flux in the phase-field model for phase l , which is responsible for preserving the finite thickness of the material interface, and this satisfies the condition $a_i(\phi_1) = -a_i(\phi_2)$. $R_{li} = \rho_l a_{li}$ is the consistent regularization flux for the mass of phase l , and $f_i = \sum_{l=1}^2 R_{li} = \sum_{l=1}^2 \rho_l a_{li}$ is the net consistent regularization flux for the mixture mass. D^* and β^* are the artificial mass diffusivity and bulk viscosity used for capturing contact discontinuity and shocks, respectively. The system of equations is discretized using a kinetic energy- and entropy-preserving second-order central scheme to capture the accurate dynamics of compressible two-phase turbulent flows.

2.1. Computation setup

The chosen setup is a compressible two-phase decaying homogeneous isotropic turbulence case. The domain consists of a triple periodic box of size $2\pi \times 2\pi \times 2\pi$, and the corresponding grid resolution of 256^3 is set such that for the initial Re_λ of 87, the corresponding $k_{\max} \eta = 1.5$, providing sufficient well-resolved results. The velocity field is initialized on the basis of an energy spectrum and is allowed to develop for 4 eddy turnover times $\tau_e = \lambda / u'$ under forcing in the incompressible version of the solver. Moreover, to avoid any transients, the drop of diameter $D = \pi/2$, with the same equation of state parameters as the carrier phase ($\gamma_l = 1.4$, $\pi_l = 0$), with turbulent Weber number of $We_t = \rho u_{\tau_{ms}}^2 D / \sigma = 0.75$ (set sufficiently low to avoid breakup), after being placed in the center of the domain continues to be forced for additional $7\tau_e$ until kinetic energy and viscous dissipation attain a steady state. Then, the compressible solver is activated at a turbulent Mach number of $Ma_t = \sqrt{\langle u_i u_i \rangle} / \langle c \rangle = 0.6$, and the turbulence is allowed to decay. Lastly, data are collected for $5\tau_e$.

Figure 1 shows the decaying nature of the compressible two-phase case, as both the kinetic energy of turbulent regions and the shocklets decay and weaken over time. Furthermore, due to the inherent transient (decay) nature of the case, statistics are collected only by spatially averaging the quantities for each snapshot. Table 1 lists the instantaneous dimensionless parameters at various times.

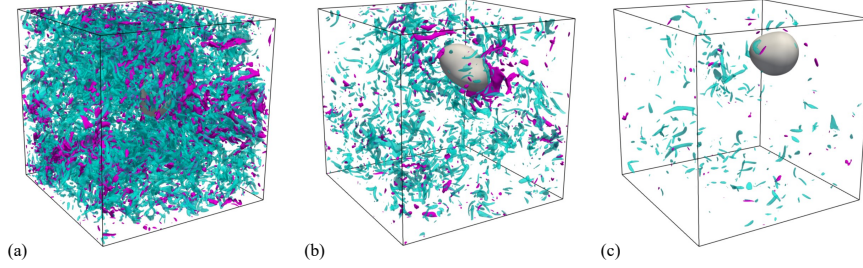


FIGURE 1. Time evolution of compressible two-phase decaying turbulence. Snapshots are presented at different times (a) $t/\tau_e = 0.5$, (b) $t/\tau_e = 2$ and (c) $t/\tau_e = 4$.

t/τ_e	Re_λ	We_t	Ma_t
0.5	80	0.6	0.55
2	75	0.4	0.45
4	67	0.3	0.35

TABLE 1. Approximate values of the dimensionless parameters at various times in the simulation.

3. Inter-scale energy transfer analysis

Prior work in the literature has used different formulations for LES of two-phase flows with respect to the continuum conservation equations. In the current work, the mathematical formulation is based on the five-equation model, which assumes one single velocity and one single pressure for both phases. Consequently, the model includes one single momentum and total energy equations, which corresponds to those used in single-phase flows with the exception of the presence of surface tension terms. Hence, the LES formalism applied to these equations is analogous to single-phase flows to a certain extent, which also applies to the resolved kinetic energy. The equation for the resolved kinetic energy for the present analyses reads

$$\frac{\partial(\bar{\rho}K_\Delta)}{\partial t} + \frac{\partial(\bar{\rho}K_\Delta \tilde{u}_j)}{\partial x_j} = - \frac{\partial}{\partial x_j} \left(\bar{p} \tilde{u}_j + \bar{\rho} \tilde{\tau}_{ij} \tilde{u}_i - \tilde{u}_i \tilde{\Sigma}_{ij} \right) - \Phi_\Delta - \Pi_\Delta + \Lambda_\Delta - D_\Delta + \Lambda_{\text{sgs}}, \quad (3.1)$$

where

$$K_\Delta = \frac{1}{2} \tilde{u}_i \tilde{u}_i, \quad \Phi_\Delta = -\bar{p} \frac{\partial \tilde{u}_j}{\partial x_j}, \quad \Pi_\Delta = -\bar{\rho} (\tilde{u}_i \tilde{u}_j - \tilde{u}_i \tilde{u}_j) \frac{\partial \tilde{u}_i}{\partial x_j}, \quad \Lambda_\Delta = \sigma \bar{\kappa} \frac{\partial \bar{\phi}}{\partial x_i} \tilde{u}_i,$$

$$D_\Delta = \tilde{\Sigma}_{ij} \frac{\partial \tilde{u}_i}{\partial x_j}, \quad \text{and} \quad \Lambda_{\text{sgs}} = \sigma \left(\bar{\kappa} \frac{\partial \bar{\phi}}{\partial x_i} - \bar{\kappa} \frac{\partial \bar{\phi}}{\partial x_i} \right) \tilde{u}_i.$$

Here, $\widetilde{(\cdot)}$ operator is the classical Favre filter defined as $\widetilde{\psi} = \bar{\rho} \bar{\psi} / \bar{\rho}$. Since the viscosities of the two phases are the same and constant, the sub-grid term arising from the nonlinearity of the viscous stress tensor disappears.

The terms in Eq. (3.1) have been rearranged in such a way that on the left-hand side we get the standard conservation form of resolved kinetic energy, whereas on the right-hand side we have a conservative transport term, which is responsible for the redistribution of

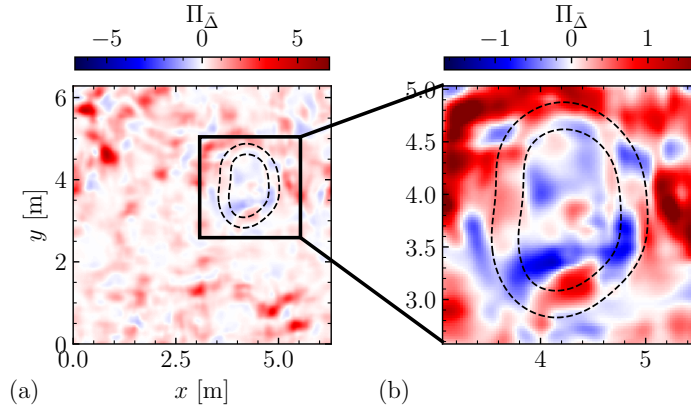


FIGURE 2. Illustration of kinetic energy flux, $\Pi_{\bar{\Delta}}$, for a filter width ratio of $\bar{\Delta}/\Delta = 17$ across (a) a x - y domain slice and (b) an area restricted to the vicinity of the interface.

energy and a series of nonconservative terms that instead act as sources and sinks of kinetic energy. In particular, the first nonconservative term is the pressure-dilatation work, hereafter denoted by $\Phi_{\bar{\Delta}}$, which is intrinsically related to the role played by compressibility in the dynamics of the resolved kinetic energy. The second term instead represents what is commonly called SGS production or the inter-scale kinetic energy flux term, $\Pi_{\bar{\Delta}}$, which is representative of the interactions between the sub-grid and resolved scales. The third term, $\Lambda_{\bar{\Delta}}$, is representative of the effects of the resolved scales on the surface tension power. The fourth term, $D_{\bar{\Delta}}$, of the viscous dissipation, which by scaling arguments is small if compared to the other terms, is thus not considered. Finally, the last term, Λ_{sgs} , corresponds to the sub-grid term arising from nonlinearity of the surface tension forces.

The present work focuses on the first three transfer terms, which are representative of the three main mechanisms of kinetic energy exchange discussed in the Section 1. Namely, pressure-dilatation work is associated with compressibility (i.e., coupling with internal energy), inter-scale kinetic energy flux (i.e., coupling with subgrid kinetic energy) and resolved surface tension power, which is linked to the surface tension forces of the resolved field (i.e., surface energy). The objective of the present work is to analyze the interplay between these different terms.

For the proposed analyses, a box filter is applied to explicitly filter the DNS data, as it was shown to produce similar results to the Gaussian filter (Wang *et al.* 2018). The filter width ratio (defined as $\bar{\Delta}/\Delta$, where $\bar{\Delta}$ is the filter width and Δ the DNS mesh size; the latter is kept constant throughout the analysis) is varied within the interval of 9 to 33 in order to assess the aforementioned energy transfers at different scales and considered single-point statistics to construct probability density functions (PDF) of the filtered data.

3.1. Inter-scale kinetic energy flux characterization

Figure 2 demonstrates the inter-scale kinetic energy transfer flux for a filter width ratio of 17 across a x - y domain slice. Positive regions of the transfer flux in red indicate the forward energy cascade, while negative regions in blue indicate the reverse cascade. Qualitatively, the mean energy flux is from the resolved to the sub-grid scales with regions of local backscatter, in agreement with single-phase results (O'Brien *et al.* 2014).

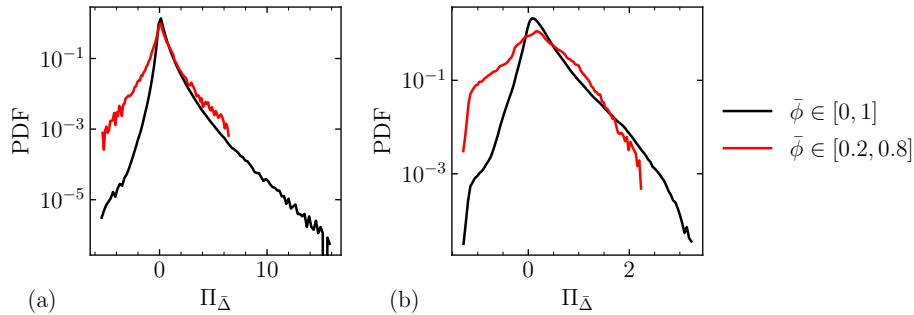


FIGURE 3. Global and conditional probability density functions of inter-scale kinetic energy flux at $Ma_t \approx 0.55$ for a filter width ratio of (a) $\bar{\Delta}/\Delta = 9$ and (b) $\bar{\Delta}/\Delta = 33$.

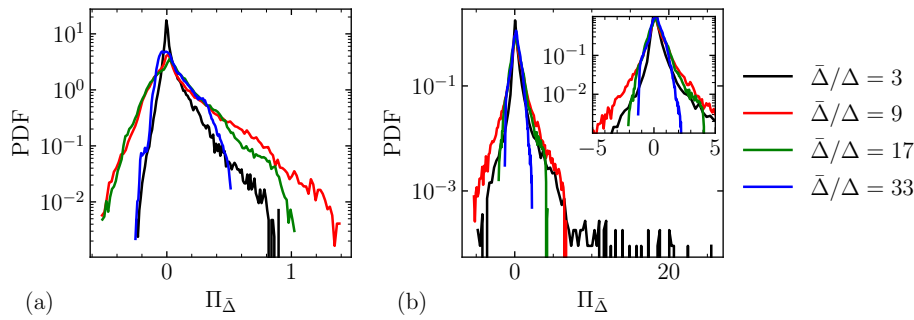


FIGURE 4. Conditional probability density functions of inter-scale kinetic energy flux for a set of filter width ratios, $\bar{\Delta}/\Delta$, from 3 to 33 at (a) $Ma_t \approx 0.35$ and (b) $Ma_t \approx 0.55$.

Moreover, Figure 3 indicates quantitatively that globally, i.e., for $\bar{\phi} \in [0, 1]$, the PDF is skewed toward the forward energy cascade from resolved to sub-grid scales for filter width ratios of 9 and 33. Furthermore, an implicit analysis of the effect of surface tension on energy transfer follows from the characterization of PDF conditioned to the interface, i.e., $\bar{\phi} \in [0.2, 0.8]$. One may observe that for both filter width ratios there is a shift in the PDF toward symmetry and an increase in values of the reverse energy cascade, namely backscatter. The increase in mean backscatter is more pronounced for the $Ma_t \approx 0.55$ snapshot. For $Ma_t \approx 0.35$, instead, this behavior occurs to a lower extent (not shown for brevity).

This first set of results indicates that locally at the interface, there is more backscatter; nevertheless, each PDF does not explicitly quantify the range of scales at which this process is more significant. Figure 4 highlights the energy transfer between resolved and sub-grid scales for different filter width ratios at different Ma_t . In both cases, for a smaller filter width ratio, sub-grid scale motions are negligible given that the grid is still rather fine and the flow sufficiently resolved. Hence, those scales close to the dissipative scales do not have enough energy to transfer up the cascade, indicated by the positive skewness of the PDF. Nevertheless, as the filter width ratio is increased to 9 and 17, the PDF's skewness decreases toward the reverse cascade, potentially indicating a range of scales at which this phenomenon might be modeled.

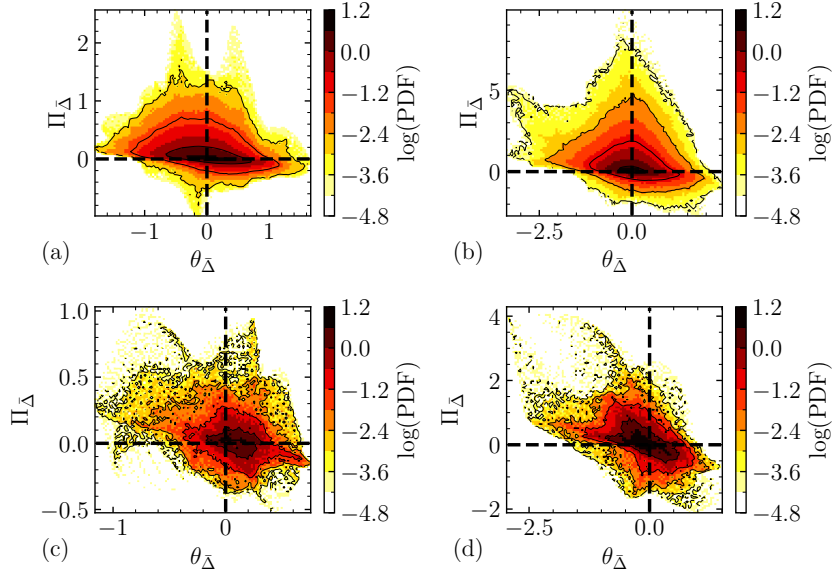


FIGURE 5. Joint probability density function (PDF) of kinetic energy flux and dilatation rate for $\bar{\Delta}/\Delta = 17$. For $\phi \in [0, 1]$, the joint PDFs correspond to the (a) $Ma_t \approx 0.35$ and (b) $Ma_t \approx 0.55$ snapshots. At the interface, i.e. $\phi \in [0.2, 0.8]$, the joint PDFs correspond to (c) $Ma_t \approx 0.35$ and (d) $Ma_t \approx 0.55$.

Thus, one may observe that in spite of the energy transfer occurring from resolved to sub-grid scales globally, and at the interface, there is an increase in the reverse cascade, which represents the implicit effect of surface tension on kinetic energy transfers. Nevertheless, for modeling purposes, the inter-scale kinetic energy flux is still unclosed; hence, by analyzing its correlation with the other resolved terms, one may propose models as functions of Ma_t , as in Wang *et al.* (2018), and We_t . This will be explored in a future study.

3.2. Correlation with pressure-dilatation work

In compressible turbulent flows, the exchange between kinetic energy and internal energy becomes more relevant in the balance. Moreover, it was observed that the pressure-dilatation term acts as a mechanism for backscatter in expansion regions (Wang *et al.* 2018; O'Brien *et al.* 2014; Tonicello *et al.* 2022). It was identified that at higher Ma_t the inter-scale kinetic energy flux becomes more correlated with dilatation rate. In particular, Wang *et al.* (2018) proposed a corresponding model for such contribution.

Figure 5 demonstrates the joint PDF of the inter-scale kinetic energy flux with the dilatation rate, again evaluated globally and conditioned at the interface, for $Ma_t \approx 0.35$ and 0.55. The Ma_t evaluated here are as close to the lower bound as are the ones studied by Wang *et al.* (2018), and by their observations, it would be expected to not see significant correlation between both quantities. Indeed, in Figure 5(a,b), the correlation is weak but increases with an increase in Ma_t . Nevertheless, even at smaller Ma_t , the correlation is stronger at the interface. Within the zone where surface tension is acting, regions of expansion ($\theta_{\bar{\Delta}} = \partial \tilde{u}_i / \partial x_i > 0$) are correlated with backscatter.

3.3. Correlation with surface tension power

Two formulations of continuum surface force are recurrent, the original one from Brackbill *et al.* (1992) in nonconservative form and one in conservative form from Gueyffier *et al.* (1999). Both are equivalent analytically, and in the DNS limit the discretized values also asymptote to the same value. The simulation was conducted with the former; however, due to its intrinsic property of enabling the splitting into a conservative transport term and nonconservative flux term, the latter is adopted in the explicit filtering analysis. Let surface tension power in the Gueyffier *et al.* (1999) form

$$u_i F_i = u_i \frac{\partial \Xi_{ij}}{\partial x_j} = \frac{\partial}{\partial x_j} (u_i \Xi_{ij}) - \Xi_{ij} \frac{\partial u_i}{\partial x_j}, \quad \text{where } \Xi_{ij} = \sigma(\delta_{ij} - n_i n_j) \delta_\Gamma, \quad (3.2)$$

where σ is the surface tension coefficient, δ_{ij} is the Kronecker delta tensor, n_i is the interface normal, and δ_Γ is the magnitude of the gradient of ϕ . Given the nonlinearity of the surface tension operator, additional SGS terms appear when filtering the momentum and, consequently, in the kinetic energy equations. However, first consider the resolved term obtained after the filtering operation to define the correspondent nonconservative flux term Λ_Δ^f in the Eq. (3.1):

$$\Lambda_\Delta^f = -\widehat{\Xi}_{ij} \frac{\partial \tilde{u}_i}{\partial x_j}. \quad (3.3)$$

Regions of high positive dilatation rate have been observed to induce the reverse cascade in highly compressible turbulent flows, and through pressure transfer energy between internal and kinetic. However, the correlation between both is seen to be stronger near the interface, potentially implying an effect of surface tension in the exchange. Furthermore, those regions of compression and expansion also interact with the surface area of the drop depending on the respective equations of state, possibly leading to changes in surface energy by the mechanism of dilatational surface tension power.

3.3.1. Surface area equation for compressible two-phase flows

An evolution equation for surface area (or surface energy) for compressible two-phase flows can be written as

$$\sigma \frac{1}{V} \frac{dA}{dt} = -\frac{1}{V} \int_\Sigma \sigma \nabla_s \cdot \mathbf{u}_s dA - \frac{1}{V} \int_V \mathbf{u} \cdot \mathbf{f}_\sigma dV, \quad (3.4)$$

where Σ is the 2D surface that represents interface, ∇_s is the surface gradient operator, \mathbf{u}_s is the velocity along the surface, and \mathbf{f}_σ is the surface tension force [see the equation for incompressible two-phase flows in Dodd & Ferrante (2016)]. Compared to the incompressible case, Eq. (3.4) has a new term (highlighted) that represents dilatation exchange; the derivation of this is deferred to the journal paper. Hence, surface tension power can also transfer energy via compressions and expansions of the flow, as well as via solenoidal velocity fluctuations. Moreover, the amount of exchange is expected to vary if the carrier and dispersed fluids are not the same (e.g., different equations of state yielding different $Ma_{t,l}$). The full picture of the energy transfer mechanisms in compressible two-phase turbulent flows is shown in Figure 6.

Figure 7 shows the dominating terms in Eq. (3.1) in proximity to the interface. Positive values of inter-scale kinetic energy transfer indicate forward cascade, positive values of the pressure-dilatation term indicate compression and positive values of surface tension power indicate removal from surface energy; the converse follows logically. One may observe that in compression regions, indeed, there is a removal of surface energy through surface

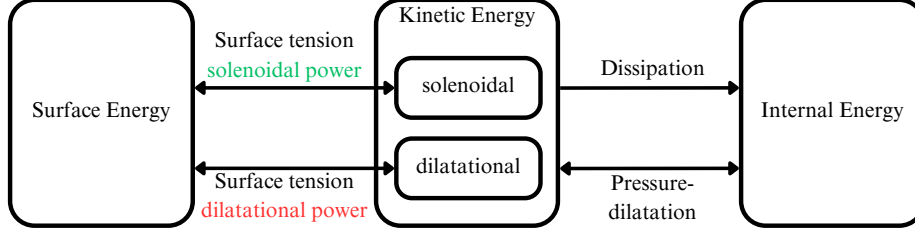
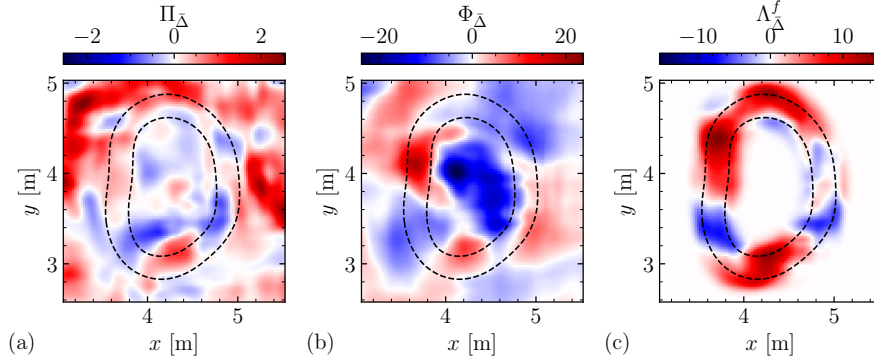


FIGURE 6. Energy transfer mechanisms in compressible two-phase turbulent flows.


 FIGURE 7. Resolved kinetic energy transfer terms for a filter width ratio of $\bar{\Delta}/\Delta = 17$: (a) kinetic energy flux, $\Pi_{\bar{\Delta}}$, (b) pressure-dilatation power, $\Phi_{\bar{\Delta}}$, and (c) resolved surface tension power, $\Lambda_{\bar{\Delta}}$.

tension power into kinetic energy and dissipation, resulting in a net forward cascade. Conversely, in expansion regions, yielding an increase in surface area, the internal energy is redistributed to kinetic energy and surface energy.

The joint PDF between inter-scale energy flux and pressure-dilatation was previously assessed and a correlation between both was observed. The correlations of inter-scale kinetic energy flux with the surface tension power source term and of pressure-dilatation with the surface tension power source term presented in Figure 8(b,c) are nontrivial. The stronger correlation between the transfer of energy between scales with the surface tension power source term is not observed, which is likely due to the intermediate role of the dilatation rate in this phenomenon and also the unknown distribution of energy into dilatational and solenoidal components. The correlation between pressure-dilatation and the surface tension power source term indicates partially that the dilatation acts as either a source or a sink of interfacial area and thus energy for a given surface tension coefficient.

4. Conclusions

A decaying compressible two-phase homogeneous isotropic turbulent case is studied to characterize the fundamental mechanisms of energy transfer in this regime, which has not been assessed before and is relevant for a diverse set of applications. Pressure-dilatation has already been shown by prior single-phase studies to be a local mechanism for the reverse energy cascade. The two-phase results corroborate that indeed on average energy is transferred from the large to the small scales; however, backscatter can still

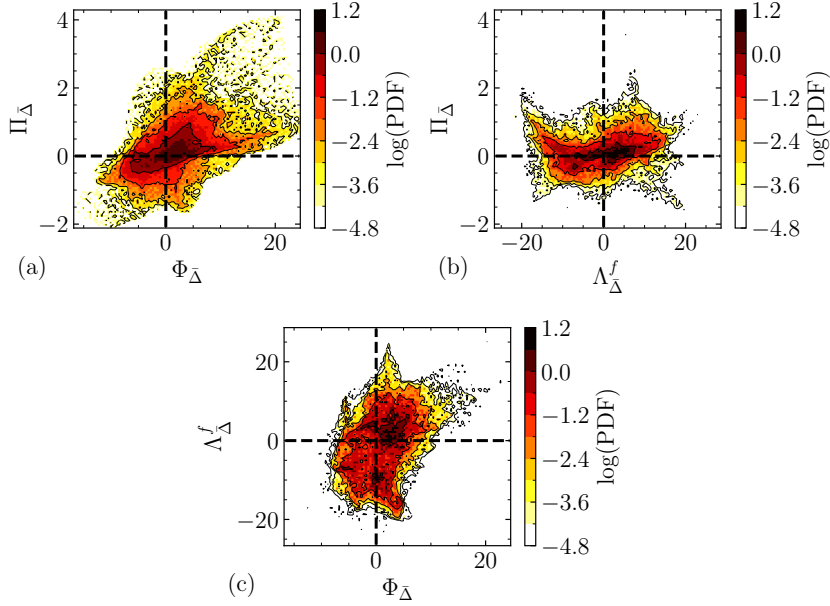


FIGURE 8. Joint probability density functions among kinetic energy flux, $\Pi_{\bar{\Delta}}$, resolved pressure-dilatation power, $\Phi_{\bar{\Delta}}$, and resolved surface tension power, $\Lambda_{\bar{\Delta}}^f$, for a filter width ratio of $\bar{\Delta}/\Delta = 17$. (a) Kinetic energy flux and resolved pressure-dilatation power, (b) kinetic energy flux and resolved surface tension power and (c) resolved surface tension power and resolved pressure-dilatation power.

occur locally and is enhanced near the interface. The main hypothesis is that dilatation introduces additional interface corrugations and thus interacts with surface area and energy (see exchange mechanisms in Figure 6). Correlations between the surface tension power source term and pressure-dilatation indicate an initial validity of this interpretation. Nevertheless, this process may not be direct, given the observations on nontrivial correlation between the inter-scale kinetic energy transfer flux and the surface tension power source term. In future studies, decomposition of the velocity into solenoidal and dilatation components, and thus kinetic energy, may enlighten these exchanges.

Acknowledgments

This research used resources of the Oak Ridge Leadership Computing Facility, which is a DOE Office of Science User Facility supported under contract DE-AC05-00OR22725. L. H. H. and S. S. J. acknowledge support from the George W. Woodruff School of Mechanical Engineering at Georgia Institute of Technology. N. T. acknowledges support from the European Union - NextGenerationEU, in the framework of the iNEST - Interconnected Nord-Est Innovation Ecosystem (iNEST ECS00000043 – CUP G93C22000610007).

REFERENCES

- ALUIE, H. 2013 Scale decomposition in compressible turbulence. *Physica D* **247**, 54–65.
 BRACKBILL, J. U., KOTHE, D. B. & ZEMACH, C. 1992 A continuum method for modeling surface tension. *J. Comput. Phys.* **100**, 335–354.

- DODD, M. S. & FERRANTE, A. 2016 On the interaction of Taylor length scale size droplets and isotropic turbulence. *J. Fluid Mech.* **806**, 356–412.
- DOMARADZKI, J. A., LIU, W. & BRACHET, M. E. 1993 An analysis of subgrid-scale interactions in numerically simulated isotropic turbulence. *Phys. Fluids* **5**, 1747–1759.
- GUEYFFIER, D., LI, J., NADIM, A., SCARDOVELLI, R. & ZALESKI, S. 1999 Volume-of-fluid interface tracking with smoothed surface stress methods for three-dimensional flows. *J. Comput. Phys.* **152**, 423–456.
- JAIN, S. S. 2022 Accurate conservative phase-field method for simulation of two-phase flows. *J. Comput. Phys.* **469**, 111529.
- JAIN, S. S., AGRAWAL, R. & MOIN, P. 2024 Stable, entropy-consistent, and localized artificial-diffusivity method for capturing discontinuities. *Phys. Rev. Fluids* **9**, 024609.
- JAIN, S. S., MANI, A. & MOIN, P. 2020 A conservative diffuse-interface method for compressible two-phase flows. *J. Comput. Phys.* **418**, 109606.
- KERR, R. M., DOMARADZKI, J. A. & BARBIER, G. 1996 Small-scale properties of non-linear interactions and subgrid-scale energy transfer in isotropic turbulence. *Phys. Fluids* **8**, 197–208.
- KLEIN, M., KETTERL, S. & HASSLBERGER, J. 2019 Large eddy simulation of multiphase flows using the volume of fluid method: part 1—governing equations and a priori analysis. *Exp. Comput. Multiph. Flow* **1**, 130–144.
- KOLMOGOROV, A. N. 1941 The local structure of turbulence in incompressible viscous fluid for very large Reynolds numbers. *Dokl. Akad. Nauk SSSR* **30**, 301.
- LABOURASSE, E., LACANETTE, D., TOUTANT, A., LUBIN, P., VINCENT, S., LEBAGUE, O., CALTAGIRONE, J.-P. & SAGAUT, P. 2007 Towards large eddy simulation of isothermal two-phase flows: governing equations and a priori tests. *Int. J. Multiph. Flow* **33**, 1–39.
- LIVESCU, D., JABERI, F. & MADNIA, C. 2002 The effects of heat release on the energy exchange in reacting turbulent shear flow. *J. Fluid Mech.* **450**, 35–66.
- LIVESCU, D. & LI, Z. 2017 Subgrid-scale backscatter after the shock-turbulence interaction. *AIP Conf. Proc.* **1793**, 150009.
- O'BRIEN, J., URZAY, J., IHME, M., MOIN, P. & SAGHAFIAN, A. 2014 Subgrid-scale backscatter in reacting and inert supersonic hydrogen-air turbulent mixing layers. *J. Fluid Mech.* **743**, 554–584.
- PIOMELLI, U., CABOT, W. H., MOIN, P. & LEE, S. 1991 Subgridscale backscatter in turbulent and transitional flows. *Phys. Fluids A* **3**, 1766–1771.
- RICHARDSON, L. F. 1922 *Weather Prediction by Numerical Process*. Cambridge University Press.
- TONICELLO, N., LODATO, G. & VERVISCH, L. 2022 Turbulence kinetic energy transfers in direct numerical simulation of shock-wave–turbulence interaction in a compression/expansion ramp. *J. Fluid Mech.* **935**, A31.
- TOUTANT, A., LABOURASSE, E., LEBAGUE, O. & SIMONIN, O. 2008 DNS of the interaction between a deformable buoyant bubble and a spatially decaying turbulence: a priori tests for LES two-phase flow modelling. *Comput. Fluids* **37**, 877–886.
- WANG, J., WAN, M., CHEN, S. & CHEN, S. 2018 Kinetic energy transfer in compressible isotropic turbulence. *J. Fluid Mech.* **841**, 581–613.